EPJ Web of Conferences **274**, 04014 (2022) https://doi.org/10.1051/epjconf/202227404014
XVth Quark Confinement and the Hadron Spectrum

Triangle Singularity in the Production of $T_{cc}^+(3875)$ and a Soft Pion at Hadron Colliders

Li-Ping He[1,*], *Eric* Braaten[2,**], *Kevin* Ingles[2,***], and *Jun* Jiang[3,****]

[1]Helmholtz-Institut für Strahlen- und Kernphysik and Bethe Center for Theoretical Physics, Universität Bonn, D-53115 Bonn, Germany
[2]Department of Physics, The Ohio State University, Columbus, OH 43210, USA
[3]School of Physics, Shandong University, Jinan, Shandong 250100, China

Abstract. If the double-charm tetraquark meson $T_{cc}^+(3875)$ is a loosely bound molecule, it can be produced in high-energy proton-proton collisions by the creation of the charm mesons $D^{*+}D^0$ at short distances followed by their binding into T_{cc}^+. It can also be produced by the creation of $D^{*+}D^{*+}$ at short distances followed by their rescattering into $T_{cc}^+\pi^+$ through a charm-meson triangle loop. A charm-meson triangle singularity produces a narrow peak in the $T_{cc}^+\pi^+$ invariant mass distribution 6.1 MeV above the threshold with a width of about 1 MeV. The fraction of T_{cc}^+ that are accompanied by π^+ with $E < m_\pi$ is estimated to be roughly 3%. The fraction of T_{cc}^+ events with $T_{cc}^+\pi^+$ in the narrow peak from the triangle singularity could be comparable.

1 Introduction

Since the discovery of $X(3872)$ (also known as $\chi_{c1}(3872)$) by the Belle Collaboration in 2003 [1], dozens of exotic hadrons containing heavy quarks have been discovered [2, 3]. The patterns of these exotic heavy hadrons are not yet understood. They present a major challenge to our understanding of QCD. The discovery of the first double-charm tetraquark meson $T_{cc}^+(3875)$ (or, more concisely, T_{cc}^+) by the LHCb Collaboration in 2021 [4] opened up a new front for exotic hadrons.

Besides $X(3872)$, the T_{cc}^+ is the other known exotic heavy hadron to which the universality of near-threshold S-wave resonances is applicable. The energy ε_T relative to the $D^{*+}D^0$ threshold measured by the LHCb Collaboration assuming a Breit-Wigner line shape is -273 ± 63 keV [4]. The real part ε_T of the pole energy assuming a line shape that takes into account the nearby $D^{*+}D^0$ threshold is [5]

$$\varepsilon_T = -360 \pm 40 \text{ keV}. \tag{1}$$

The analysis by the LHCb Collaboration suggests that its J^P quantum numbers are 1^+. This implies that T_{cc}^+ has an S-wave coupling to $D^{*+}D^0$. Universality of near-threshold S-wave resonance indicates the dominant component of the wavefunction of T_{cc}^+ is a loosely bound

*e-mail: heliping@hiskp.uni-bonn.de
**e-mail: braaten.1@osu.edu
***e-mail: ingles.27@buckeyemail.osu.edu
****e-mail: jiangjun87@sdu.edu.cn

© The Authors, published by EDP Sciences. This is an open access article distributed under the terms of the Creative Commons Attribution License 4.0 (http://creativecommons.org/licenses/by/4.0/).

$D^{*+}D^0$ molecule. However, universality says nothing about the wavefunction at shorter distances. The wavefunction of T_{cc}^+ at shorter distances has a small $D^{*0}D^+$ component. It could also have a compact tetraquark component ($cc\bar{q}\bar{q}$) or a component with $\bar{q}\bar{q}$ bound to a heavy diquark (cc). Since its discovery, there have been numerous studies of the T_{cc}^+ tetraquark. We refer to Ref. [3] and references therein for other studies.

In this proceeding, we review the triangle singularity in the production of T_{cc}^+ and a soft pion based on Ref. [6]. A *triangle singularity* is a kinematic singularity that arises if three virtual particles that form a triangle in a Feynman diagram can all be on their mass shells simultaneously [7, 8]. It provides a possible way to reveal the nature of a hadron through its production. The triangle singularity produces a double-log divergence in a reaction rate. For the production of $T_{cc}^+\pi^+$, the divergence is smoothed out into a narrow peak by the binding energy of the molecule and by the decay widths of the charm mesons in the triangle. The effects of triangle singularities on the production of exotic heavy mesons has been studied in Refs. [9–11]. More applications can be found in Ref. [12].

2 $T_{cc}^+(3875)$ as a loosely bound S-wave molecule

The extremely small energy of T_{cc}^+ relative to the $D^{*+}D^0$ threshold suggests that the T_{cc}^+ must be a loosely bound molecule dominated by the $D^{*+}D^0$ component. The few-body physics of charm mesons has universal aspects that are determined by their *binding momentum* $\gamma_T = \sqrt{2\mu|\varepsilon_T|}$ or *scattering length* $1/\gamma_T$ [13], where μ is their reduced mass. Given the energy ε_T of T_{cc}^+ in Eq. (1), its binding momentum is $\gamma_T = 26.4 \pm 1.5$ MeV. The mean separation of the charm mesons is $\langle r \rangle = 1/(2\gamma_T) = 3.7 \pm 0.2$ fm, which is almost an order of magnitude larger than the radius of most hadrons.

2.1 Universal wavefunction

The normalized universal momentum-space wavefunction for the charm-meson molecule is

$$\psi_T(k) = \sqrt{8\pi\gamma_T}/(k^2 + \gamma_T^2). \tag{2}$$

The spatial wavefunction at the origin $\psi(r=0) = \int d^3k\, \psi(k)/(2\pi)^3$ is ultraviolet divergent: it can be regularized by imposing a sharp momentum cutoff $|\boldsymbol{k}| < (\pi/2)\Lambda$ with $\Lambda \gg \gamma_T$. The resulting expression, up to corrections that go to 0 as $\Lambda \to \infty$, is

$$\psi_T(r=0) = (\Lambda - \gamma_T)\sqrt{\gamma_T/2\pi}. \tag{3}$$

The ultraviolet cutoff Λ can be interpreted as the momentum scale beyond which $\psi_T(k)$ decreases more rapidly than the prediction $1/k^2$ from the universal wavefunction in Eq. (2). An order-of-magnitude estimate for the ultraviolet cutoff Λ is the pion mass m_π. The wavefunction at the origin can be used to take into account short-distance components of the bound state that are not described explicitly.

2.2 Model wavefunction at shorter distances

A sharp ultraviolet cutoff on the momentum $\boldsymbol{k}$ for the universal wavefunction gives unphysical results for some observables. A simple model wavefunction that gives the same momentum dependence as the universal wavefunction $\psi_T(k)$ at small k and a more physical qualitative behavior at large k, or equivalently at short distances, is

$$\psi_T^{(\Lambda)}(k) = \sqrt{8\pi(\Lambda+\gamma_T)\Lambda\gamma_T}/(\Lambda-\gamma_T)\left[\left(k^2+\gamma_T^2\right)^{-1} - \left(k^2+\Lambda^2\right)^{-1}\right]. \tag{4}$$

This regularized wavefunction was first applied to $X(3872)$ by Suzuki [14]. The spatial wavefunction at the origin is

$$\psi_T^{(\Lambda)}(r=0) = \sqrt{(\Lambda+\gamma_T)\Lambda\gamma_T/2\pi}. \tag{5}$$

2.3 Model wavefunction for coupled channel

The scattering threshold of $D^{*0}D^+$ is higher than that of $D^{*+}D^0$ by $\delta = +1.41 \pm 0.03$ MeV. Hence, the T_{cc}^+ would also have a $D^{*0}D^+$ component with a smaller probability. We denote this coupled channel simply by 0+. The binding energy and binding momentum of T_{cc}^+ for the $D^{*0}D^+$ channel are $\delta + |\varepsilon_T| = 1.77 \pm 0.05$ MeV and $\gamma_{0+} = \sqrt{2\mu(\delta+|\varepsilon_T|)} = 58.5 \pm 0.8$ MeV.

We will assume that at short distances, the T_{cc}^+ is in the isospin-0 combination $(D^{*+}D^0 - D^{*0}D^+)/\sqrt{2}$ of the two coupled channels. This is consistent with the observation by the LHCb Collaboration [4, 5]. The two channels are related by isospin symmetry that is broken by the energy difference δ. We assume the symmetry requires the wavefunctions in the two channels to be equal at short distances: $\psi_{0+}^{(\Lambda)}(r=0) = \psi_T^{(\Lambda)}(r=0)$. Therefore, the regularized wavefunction for the $D^{*0}D^+$ channel is

$$\psi_{0+}^{(\Lambda)}(k) = \sqrt{8\pi(\Lambda+\gamma_T)\Lambda\gamma_T}/(\Lambda-\gamma_{0+})\left[\left(k^2+\gamma_{0+}^2\right)^{-1} - \left(k^2+\Lambda^2\right)^{-1}\right]. \tag{6}$$

Its corresponding relative probability is

$$Z_{0+} \equiv \int d^3k/(2\pi)^3 \left|\psi_{0+}^{(\Lambda)}(k)\right|^2 = \frac{(\Lambda+\gamma_T)\gamma_T}{(\Lambda+\gamma_{0+})\gamma_{0+}}. \tag{7}$$

This is less than 1 provided γ_T is smaller than γ_{0+}.

We introduce a coupled-channel model defined by the regularized wavefunctions in Eqs. (4) and (6), whose behavior is more physical at large momentum. In this model, the two components of the coupled channel are described explicitly and all others are taken into account through the wavefunction at the origin. The total probability in the two channels can be normalized to 1 by multiplying both $\psi_T^{(\Lambda)}(k)$ in Eq. (4) and $\psi_{0+}^{(\Lambda)}(k)$ in Eq. (6) by $1/\sqrt{1+Z_{0+}}$.

3 XEFT for the double-charm sector

An appropriate effective field theory that provides a systematically improvable treatment of the near-threshold S-wave resonance was invented by Fleming *et al.* [15]. It was originally used to describe $D^*\bar{D}$, $D\bar{D}^*$, $D\bar{D}\pi$, or $X(3872)$ with total energy near the $D^*\bar{D}$ threshold. Thus, it is generally called XEFT. It is a nonrelativistic effective field theory for charm mesons $D^{(*)}$ and $\bar{D}^{(*)}$ and pions π. A Galilean-invariant formulation of XEFT that exploits the approximate conservation of mass in the transitions $D^* \leftrightarrow D\pi$ was introduced in Ref. [16] and further developed in Ref. [17]. XEFT can equally well be applied to T_{cc}^+ and its meson constituents. It can describe D^*D, $DD\pi$, and T_{cc}^+ with total energy near the D^*D thresholds. It can also be applied to D^*D^*, $D^*D\pi$, $DD\pi\pi$, and $T_{cc}^+\pi$ with total energy near the D^*D^* thresholds [18].

In Sec. 2.3, we introduced the coupled-channel model for the loosely bound charm-meson molecule T_{cc}^+. If an amplitude in XEFT for producing T_{cc}^+ is in a form with a factor of the universal wavefunction $\psi_T(k)$ in Eq. (2), then the corresponding amplitudes for the two coupled channels can be obtained by making the substitutions

$$\psi_T(k) \longrightarrow \psi_T^{(\Lambda)}(k)/\sqrt{1+Z_{0+}}, \qquad \psi_{0+}(k) \longrightarrow -\psi_{0+}^{(\Lambda)}(k)/\sqrt{1+Z_{0+}}. \tag{8}$$

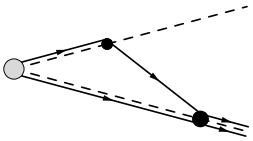

Figure 1. Feynman diagram in XEFT for D^*D^* created at a point to rescatter into $T_{cc}^+\pi$. The π, D, D^* and T_{cc}^+ are represented by a dashed line, a solid line, a double (solid+dashed) line, and a triple (solid+dashed+solid) line, respectively.

4 Production of T_{cc}^+ and a soft pion

4.1 Triangle-singularity peaks from $D^{*+}D^0$ channel

4.1.1 Amplitude for $T_{cc}^+\pi^a$

As a loosely bound molecule, T_{cc}^+ can be produced by the rescattering of its charm-meson constituents D^{*+} and D^0. It can also be produced together with a pion π^a ($a = +, 0$) by the rescattering of $D^{*+}D^{*a}$ created at short distances. The corresponding Feynman diagram in XEFT is shown in Fig. 1. The blob on the left side is the vertex factor $i\,\mathcal{A}^{ij}_{D^{*+}D^{*a}+y}$ for creating $D^{*+}D^{*a}$ at a point while producing additional particles y with large momenta in the $D^{*+}D^{*a}$ center-of-momentum (CM) frame. The amplitude for producing $T_{cc}^+\pi^a$ is

$$\mathcal{A}_{T_{cc}^+\pi^a+y}(\boldsymbol{q}) = -G_\pi^a\,\sqrt{\gamma_T}\,\mathcal{A}^{ij}_{D^{*+}D^{*a}+y}\varepsilon^{i*}q^j\,T_a(q^2,\gamma). \tag{9}$$

where $\boldsymbol{q}$ is the relative momentum of $T_{cc}^+\pi^a$ in their CM frame, $\boldsymbol{\varepsilon}$ is the polarization vector for T_{cc}^+ and G_π^a is a constant that satisfies $G_\pi^+/G_\pi^0 = \sqrt{2}$. The triangle amplitude $T_a(q^2,\gamma)$ depends on the charge of the outgoing pion and its two arguments: q^2 and the complex binding momentum $\gamma = \sqrt{-2\mu(\varepsilon_T + i\,\Gamma_{*+}/2)}$, where $\Gamma_{*+} = 83$ keV is the D^{*+} total decay width. It is convenient to express the triangle amplitude in terms of the total kinetic energy $E = q^2/(2\mu_{\pi T})$ of $T_{cc}^+\pi^a$:

$$T_a(q^2,\gamma) = A_a(q^2,\gamma)\log\frac{\sqrt{M_*(E-E_a)} + \sqrt{(M_*m/M_T)E} + i\gamma}{\sqrt{M_*(E-E_a)} - \sqrt{(M_*m/M_T)E} + i\gamma} + \frac{1}{M_*E}\left(\sqrt{M_*(E-E_a)} - i\gamma\right), \tag{10}$$

where we denote m, M, $M_* = M + m$, and $M_T = M_* + M$ as the kinetic masses of π^a, D^a, D^{*a}, and T_{cc}^+ in Galilean-invariant XEFT, respectively. Their corresponding physical masses can be denoted by adding an additional subscript a to distinguish among different isospin states. The coefficient of the logarithmic term is denoted as $A_a(q^2,\gamma)$. The complex constant E_a is

$$E_a = M_{*a} - M_0 - m_a - \varepsilon_T - i\,(\Gamma_{*+} + \Gamma_{*a})/2. \tag{11}$$

In the limit $\Gamma_{*a} \to 0$, E_a is real: $E_+^{\rm lim} = 5.9$ MeV $- \varepsilon_T$ and $E_0^{\rm lim} = 7.0$ MeV $- \varepsilon_T$.

The triangle amplitude $T_a(q^2,\gamma^2)$ has a square-root branch point at $E = E_a$ from the square-root terms in Eq. (10). It also has a logarithmic branch point at

$$E_{\triangle a} = M_*/(4\mu^2)\left(\sqrt{2\mu E_a - \gamma^2} - i\,\sqrt{m/M_T}\,\gamma\right)^2, \tag{12}$$

which can be determined by setting the denominator of the argument of the logarithmic term to 0. This is the *triangle singularity* that happens when the three charm-meson lines that form a triangle in Fig. 1 are all simultaneously on shell. The two charm mesons that connect T_{cc}^+ can both be on shell in the limit as the binding energy goes to 0. The other one in the triangle can be brought on shell by tuning the momentum of the outgoing pion. In the limits $\varepsilon_T \to 0$ and $\Gamma_{*a} \to 0$, the complex triangle-singularity energy $E_{\triangle a}$ goes to a real constant: $E_{\triangle a} \to (M_T/2M)(M_{*a} - M_0 - m_a)$, whose limiting values are $E_{\triangle+}^{\rm lim} = 6.1$ MeV and $E_{\triangle 0}^{\rm lim} = 7.3$ MeV.

4.1.2 Cross section for $T_{cc}^+\pi^a$

The differential cross sections for $T_{cc}^+\pi^+$ and $T_{cc}^+\pi^0$ as functions of E are

$$\frac{d\sigma}{dE}[T_{cc}^+\pi^+] = \left\langle \mathcal{A}_{D^+D^0}(\mathcal{A}_{D^+D^0})^* \right\rangle \frac{(G_\pi^+)^2\gamma_T}{\pi^2}(2\mu_{\pi T}E)^{3/2}\left|T_+(2\mu_{\pi T}E,\gamma)\right|^2, \tag{13a}$$

$$\frac{d\sigma}{dE}[T_{cc}^+\pi^0] = \left\langle \mathcal{A}_{D^+D^0}(\mathcal{A}_{D^+D^0})^* \right\rangle \frac{3(G_\pi^0)^2\gamma_T}{4\pi^2}(2\mu_{\pi T}E)^{3/2}\left|T_0(2\mu_{\pi T}E,\gamma)\right|^2, \tag{13b}$$

where we have expressed both cross sections in terms of the same short-distance factor $\langle \mathcal{A}_{D^+D^0}(\mathcal{A}_{D^+D^0})^* \rangle$ that appears in the cross section for T_{cc}^+ produced from the rescattering of $D^{*+}D^0$.

In the simultaneous limits $\varepsilon_T \to 0$ and $\Gamma_{*a} \to 0$, the differential cross section has a $\log^2$ divergence at $E_{\triangle a}^{\rm lim}$ caused by the triangle singularity (case (d) in Fig. 2). In the limit $\Gamma_{*a} \to 0$, $d\sigma/dE$ develops a cusp at $E_a^{\rm lim}$. For $|\varepsilon_T| = 360$ keV (case (b) in Fig. 2), the cusp coincides with the peak. For $\varepsilon_T = 0$ (case (d) in Fig. 2), the cusp at $E_+^{\rm lim} = 5.9$ MeV is well separated from the $\log^2$ divergence at 6.1 MeV from the triangle singularity.

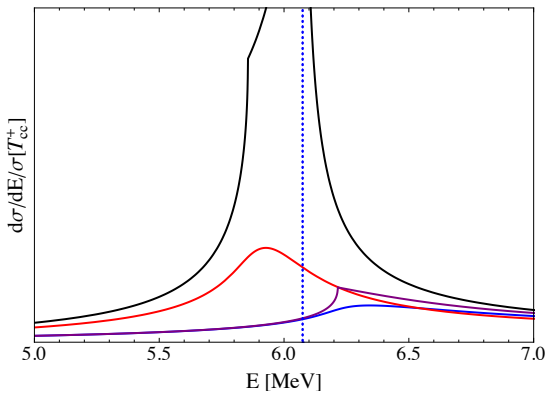

Figure 2. Differential cross sections $d\sigma[T_{cc}^+\pi^+]/dE$ divided by $\sigma[T_{cc}^+, \text{no}\,\pi]$ as functions of the invariant kinetic energy E. The four cases of $(|\varepsilon_T|, \Gamma_{*+})$ in order of increasing height of the peak are (a) (360 keV, 83 keV) (blue curve), (b) (360 keV, 0) (purple curve), (c) (0, 83 keV) (red curve), and (d) (0, 0) (black curve). The vertical dotted line is at the limiting triangle-singularity energy $E_{\triangle+}^{\rm lim}$. The scale on the vertical axis is arbitrary.

At physical values of the decay widths Γ_{*a}, the differential cross sections $d\sigma/dE$ for $T_{cc}^+\pi^+$ and $T_{cc}^+\pi^0$ are illustrated in Fig. 3 for three values of the T_{cc}^+ binding energy: $|\varepsilon_T| = 320$, 360, and 400 keV. The differential cross sections for $T_{cc}^+\pi^+$ and $T_{cc}^+\pi^0$ each has a narrow peak near the limiting triangle-singularity energy $E_{\triangle a}^{\rm lim}$. The full width at half maximum of the peak is about 1 MeV. As $|\varepsilon_T|$ decreases, the energy at the peak approaches the limiting triangle-singularity energy $E_{\triangle a}^{\rm lim}$. It decreases through that energy when $|\varepsilon_T|$ decreases below about 0.1 MeV. The shape of $d\sigma/dE$ near the peak is determined by the interplay between the logarithmic singularity and the square-root singularity in the triangle amplitude.

4.2 Coupled-channel model

4.2.1 Cross sections

The cross sections in Eqs. (13) increase asymptotically as $E^{1/2}$ at large E. This unphysical behavior is an artifact of using the universal approximation for T_{cc}^+ beyond its range of applicability. The coupled-channel model introduced in Section 2.3 is a simple model with universal behavior at long distances and a more physical qualitative behavior at short distances. The model gives predictions for the production of not only $T_{cc}^+\pi^+$ and $T_{cc}^+\pi^0$, but $T_{cc}^+\pi^-$ as well.

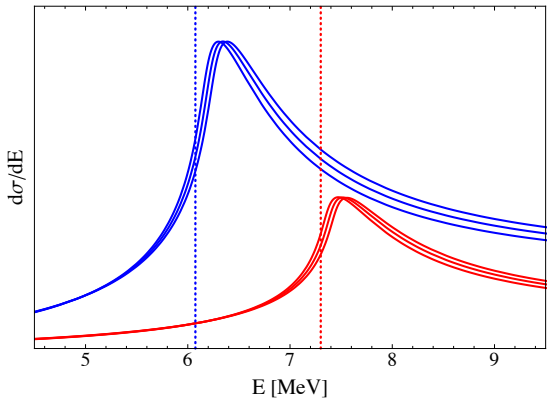

Figure 3. Differential cross sections $d\sigma/dE$ from Eqs. (13) as functions of the invariant kinetic energy E for $T_{cc}^+\pi^+$ (left blue curves) and for $T_{cc}^+\pi^0$ (right red curves). The binding energies of T_{cc}^+ are 320, 360, and 400 keV in order of increasing energy at the peak. The vertical dotted lines are at the limiting triangle-singularity energies $E_{\triangle a}^{\rm lim}$. The scale on the vertical axis is arbitrary.

The differential cross sections for $T_{cc}^+\pi^+$, $T_{cc}^+\pi^0$, and $T_{cc}^+\pi^-$ in the coupled-channel model as functions of the invariant kinetic energy E are

$$\frac{d\sigma}{dE}[T_{cc}^+\pi^+] = \left\langle \mathcal{A}_{D^+D^0}(\mathcal{A}_{D^+D^0})^* \right\rangle \frac{(G_\pi^+)^2\gamma_T}{\pi^2}(2\mu_{\pi T}E)^{3/2}\left|T_+^{(\Lambda)}(2\mu_{\pi T}E,\gamma)\right|^2, \tag{14a}$$

$$\frac{d\sigma}{dE}[T_{cc}^+\pi^0] = \left\langle \mathcal{A}_{D^+D^0}(\mathcal{A}_{D^+D^0})^* \right\rangle \frac{3(G_\pi^0)^2\gamma_T}{4\pi^2}(2\mu_{\pi T}E)^{3/2} \times\left(\left|T_0^{(\Lambda)}(2\mu_{\pi T}E,\gamma)\right|^2 + \left|T_0'^{(\Lambda)}(2\mu_{\pi T}E,\gamma_{0+})\right|^2\right), \tag{14b}$$

$$\frac{d\sigma}{dE}[T_{cc}^+\pi^-] = \left\langle \mathcal{A}_{D^+D^0}(\mathcal{A}_{D^+D^0})^* \right\rangle \frac{(G_\pi^+)^2\gamma_T}{\pi^2}(2\mu_{\pi T}E)^{3/2}\left|T_-'^{(\Lambda)}(2\mu_{\pi T}E,\gamma_{0+})\right|^2. \tag{14c}$$

The regularized triangle amplitudes $T_a^{(\Lambda)}$ and $T_{a'}'^{(\Lambda)}$ with $a' = \{0,-\}$ are deduced by using the substitutions in Eq. (8). The differential cross sections $d\sigma/dE$ are shown in Fig. 4. The triangle-singularity peaks for $T_{cc}^+\pi^+$ and $T_{cc}^+\pi^0$ in the coupled-channel model have essentially the same shape as those with the universal triangle amplitudes. There is no triangle singularity in the production of $T_{cc}^+\pi^-$, because the mass of D^{*0} is 2.4 MeV below the threshold for the decay into $D^+\pi^-$. This prevents the D^{*0} and D^+ lines in the triangle diagram from being simultaneously on shell. The height of the peak for $T_{cc}^+\pi^+$ in the coupled-channel model is smaller by the multiplicative factor $1/(1+Z_{0+})$. The height of the peak for $T_{cc}^+\pi^0$ in the coupled-channel model is approximately equal to that with the universal triangle amplitude. This is the result of a fortuitous compensation between the multiplicative factor $1/(1+Z_{0+})$ and the additional contribution from the $D^{*0}D^+$ component of T_{cc}^+.

At energies above the peaks, there is a significant decrease in all three cross sections as Λ decreases. The dependence on Λ demonstrates that the cross sections above the triangle-singularity peaks are model dependent.

4.2.2 High energy limits

The differential cross sections for $T_{cc}^+\pi^+$, $T_{cc}^+\pi^0$, and $T_{cc}^+\pi^-$ in Eqs. (14) all decrease asymptotically as $E^{-1/2}$ at large E. The cross sections integrated up to an energy $E_{\rm max}$ much larger than the limiting triangle-singularity energies can be expressed as

$$\sigma[T_{cc}^+\pi^+] \approx \left(3.2\sqrt{E_{\rm max}/m_\pi} - 0.0^{+1.8}_{-1.3}\right)\times 10^{-2}\,\sigma^{(\Lambda)}[T_{cc}^+,{\rm no}\,\pi], \tag{15a}$$

$$\sigma[T_{cc}^+\pi^0] \approx \left(2.4\sqrt{E_{\rm max}/m_\pi} - 0.0^{+1.3}_{-1.0}\right)\times 10^{-2}\,\sigma^{(\Lambda)}[T_{cc}^+,{\rm no}\,\pi], \tag{15b}$$

$$\sigma[T_{cc}^+\pi^-] \approx \left(3.2\sqrt{E_{\rm max}/m_\pi} - 1.3^{+0.3}_{-0.5}\right)\times 10^{-2}\,\sigma^{(\Lambda)}[T_{cc}^+,{\rm no}\,\pi]. \tag{15c}$$

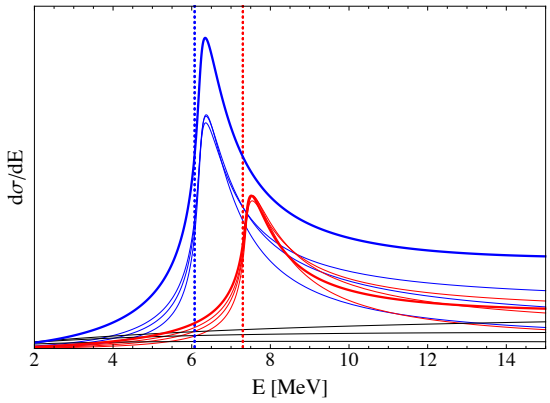

Figure 4. $d\sigma/dE$ for $T_{cc}^+\pi^+$ (left blue curves), $T_{cc}^+\pi^0$ (right red curves), and $T_{cc}^+\pi^-$ (lower black curves). The binding energy of T_{cc}^+ is $|\varepsilon_T| = 360$ keV. The thicker curves for $T_{cc}^+\pi^+$ and $T_{cc}^+\pi^0$ were calculated using Eqs. (13). The thinner curves are for the coupled-channel model with $\Lambda/m_\pi = 1/2$, 1, and 2 in order of increasing cross sections at small E and at large E.

The coefficients of $\sqrt{E_{\rm max}/m_\pi}$ were determined from the asymptotic behaviors of $d\sigma/dE$. The numerical coefficients with error bars were deduced by fitting the subleading behavior at large $E_{\rm max}$ with $\Lambda = 2^{0\pm1} m_\pi$.

In experimental measurements of $d\sigma/dE$ for $T_{cc}^+\pi^+$, subtracting $d\sigma/dE$ for $T_{cc}^+\pi^-$ would also remove the background from random pions from the pp collision that have nothing to do with the creation of charm mesons. The difference between the cross sections in the coupled-channel model in Eqs. (14a) and (14c) is shown as a function of E in Fig. 5. The difference between their integrated cross sections is independent of $E_{\rm max}$:

$$\sigma[T_{cc}^+\,\pi^+] - \sigma[T_{cc}^+\,\pi^-] \approx \left(1.3^{+1.5}_{-0.8}\right) \times 10^{-2}\, \sigma^{(\Lambda)}[T_{cc}^+, \text{no}\,\pi]\,. \tag{16}$$

We can use this difference as an estimated contribution for $T_{cc}^+\,\pi^+$ from the triangle-singularity peak, because it is dominated by the peak.

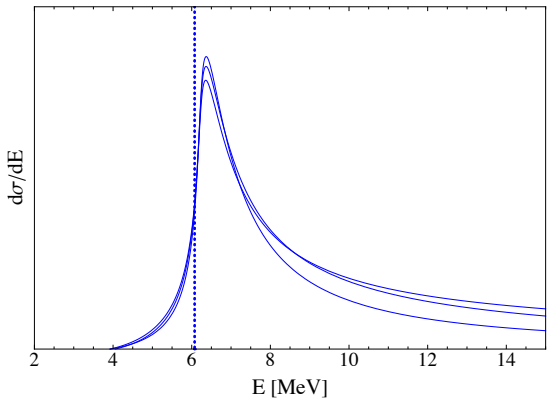

Figure 5. Difference between the differential cross sections $d\sigma/dE$ for $T_{cc}^+\pi^+$ and $T_{cc}^+\pi^-$ in the coupled-channel model as functions of the invariant kinetic energy E. The binding energy of T_{cc}^+ is $|\varepsilon_T| = 360$ keV. The curves were calculated using Eqs. (14a) and (14c) with $\Lambda/m_\pi = 1/2$, 1, and 2 in order of increasing cross sections at small E and at large E.

4.3 LHCb data

The inclusive cross section for T_{cc}^+ is the sum of the cross section $\sigma^{(\Lambda)}[T_{cc}^+, \text{no}\,\pi]$ for T_{cc}^+ without any pion and the cross sections $\sigma[T_{cc}^+\pi^\pm]$ and $\sigma[T_{cc}^+\pi^0]$. At a hadron collider, it is much easier to detect a charged pion than a neutral pion. The fractions of events having $T_{cc}^+\pi^+$ and $T_{cc}^+\pi^-$ with invariant kinetic energy less than m_π are estimated to be $(3.0^{+1.5}_{-1.2})\%$ and $(1.8^{+0.2}_{-0.4})\%$, respectively. The fraction of events from the triangle-singularity peak for $T_{cc}^+\pi^+$ can be estimated using the result in Eq. (16): $(1.2^{+1.3}_{-0.7})\%$. The LHCb has observed 117 ± 16

T_{cc}^+ events [4, 5]. Our estimate suggests that a few of the T_{cc}^+ events observed by the LHCb Collaboration could have a π^+ in the peak from the triangle singularity. While the number of these events is small, they all have invariant kinetic energy E of $T_{cc}^+\pi^+$ within 1 MeV of 6.1 MeV. The creation of charm mesons at short distances should produce essentially no $T_{cc}^+\pi^-$ events in that region of E. The production of $T_{cc}^+\pi^-$ can therefore be used to measure the background from $T_{cc}^+\pi^+$ events with a random π^+ from the pp collision.

5 Summary

In summary, the charm-meson triangle singularity produces narrow peaks in the production of T_{cc}^+ and a soft pion. The narrow peak is near 6.1 MeV for $T_{cc}^+\pi^+$ and 7.3 MeV for $T_{cc}^+\pi^0$. We also introduced a coupled-channel model for the $D^{*+}D^0$ and $D^{*0}D^+$ components of T_{cc}^+ with isospin symmetry at short distances. The differential cross section $d\sigma/dE$ for producing $T_{cc}^+\pi^+$ is predicted to decrease as $E^{-1/2}$ at large energy. This behavior provides a way of discriminating between a loosely bound charm-meson molecule and a compact tetraquark.

Our estimate of the cross section for $T_{cc}^+\pi^+$ from the triangle-singularity peak is large enough to encourage the effort to observe the peak at the LHC. The observation of such a peak would provide strong support for the identification of T_{cc}^+ as a loosely bound charm-meson molecule.

Acknowledgements

This work was supported in part by the U.S. Department of Energy under grant DE-SC0011726, by the National Natural Science Foundation of China (NSFC) under grant 11905112, by the Alexander von Humboldt Research Foundation, and by the NSFC and the Deutsche Forschungsgemeinschaft (DFG) through the Sino-German Collaborative Research Center TRR110 (NSFC grant 12070131001, DFG Project-ID 196253076-TRR110).

References

[1] S. Choi et al. (Belle), Phys. Rev. Lett. **91**, 262001 (2003), hep-ex/0309032
[2] N. Brambilla, S. Eidelman, C. Hanhart, A. Nefediev, C.P. Shen, C.E. Thomas, A. Vairo, C.Z. Yuan, Phys. Rept. **873**, 1 (2020), 1907.07583
[3] H.X. Chen, W. Chen, X. Liu, Y.R. Liu, S.L. Zhu (2022), 2204.02649
[4] R. Aaij et al. (LHCb), Nature Phys. **18**, 751 (2022), 2109.01038
[5] R. Aaij et al. (LHCb), Nature Commun. **13**, 3351 (2022), 2109.01056
[6] E. Braaten, L.P. He, K. Ingles, J. Jiang, Phys. Rev. D **106**, 034033 (2022), 2202.03900
[7] R. Karplus, C.M. Sommerfield, E.H. Wichmann, Phys. Rev. **111**, 1187 (1958)
[8] L.D. Landau, Nucl. Phys. **13**, 181 (1959)
[9] A.P. Szczepaniak, Phys. Lett. B **747**, 410 (2015), 1501.01691
[10] X.H. Liu, M. Oka, Q. Zhao, Phys. Lett. B **753**, 297 (2016), 1507.01674
[11] L. He, K. Ingles, E. Braaten, J. Jiang, PoS **CHARM2020**, 027 (2021)
[12] F.K. Guo, X.H. Liu, S. Sakai, Prog. Part. Nucl. Phys. **112**, 103757 (2020), 1912.07030
[13] E. Braaten, H.W. Hammer, Phys. Rept. **428**, 259 (2006), cond-mat/0410417
[14] M. Suzuki, Phys. Rev. D **72**, 114013 (2005), hep-ph/0508258
[15] S. Fleming, M. Kusunoki, T. Mehen, U. van Kolck, Phys. Rev. D **76**, 034006 (2007), hep-ph/0703168
[16] E. Braaten, Phys. Rev. D **91**, 114007 (2015), 1503.04791
[17] E. Braaten, L.P. He, J. Jiang, Phys. Rev. D **103**, 036014 (2021), 2010.05801
[18] E. Braaten, H.W. Hammer, T. Mehen, Phys. Rev. D **82**, 034018 (2010), 1005.1688